

AMSU-A land surface emissivity estimation for numerical weather prediction assimilation schemes

Catherine Prigent

Corresponding author: Centre National de la Recherche Scientifique, Laboratoire d'Etudes du Rayonnement et de la Matière en Astrophysique, Observatoire de Paris, 61, avenue de l'Observatoire, Paris, France. Tel: 33 (0) 1 40 51 20 18. Fax: 33 (0) 1 40 51 20 02. (catherine.prigent@obspm.fr)

Frédéric Chevallier

European Centre for Medium-range Weather Forecasts, Reading, UK; Now at Centre National de la Recherche Scientifique, Laboratoire des Sciences du Climat et l'Environnement, Gif-sur-Yvette, France

Fatima Karbou

Centre National de la Recherche Scientifique, Centre d'étude des Environnements Terrestre et Planétaires, Vélizy, France.

Peter Bauer, and Graeme Kelly

European Centre for Medium-range Weather Forecasts, Reading, UK.

Short title: AMSU-A LAND SURFACE EMISSIVITY

Abstract. This study describes the work performed at ECMWF to estimate the microwave land surface emissivities at AMSU-A frequencies, within the specific context and constraint of operational assimilation. The emissivities are directly calculated from the satellite observations in clear sky condition, using the surface skin temperature derived from ECMWF and the RTTOV radiative transfer model along with the forecast model variables to estimate the atmospheric contributions. The results are analyzed, with special emphasis on the evaluation of the frequency and angular dependencies of the emissivities with respect to the surface characteristics. Possible extrapolation of the SSM/I emissivities to the AMSU ones is considered. Direct calculation results are also compared with emissivity model outputs.

1. Introduction

Since 1998, the Advanced Microwave Sounding Unit - A (AMSU-A) on board the National Oceanic and Atmospheric Administration (NOAA) polar orbiters provide unique atmospheric temperature profiling capabilities, both in the troposphere and in the stratosphere. Exploiting this data has been a key challenge for numerical weather prediction (NWP) centers (e.g., English et al 2000, Kelly and Bauer 2000).

Several factors contribute to make assimilation of such data more difficult over land than over ocean. Microwave land surface emissivities are usually much higher than ocean emissivities, making the surface contribution larger. They have also a shorter spatial correlation scale. In addition, they are very complex to model, from arid surfaces to dense vegetation or snow, being dependent on a large number of highly variable parameters. The impact of the emissivity errors on the atmospheric temperature and humidity retrievals has been analyzed by English (2000). Efforts have been directed toward a better understanding of the mechanisms responsible for the microwave emission of continental surfaces, from both theoretical analysis and field experiments. Model developments include detailed simulations of bare soil (e.g., Shi et al. 2002), vegetation canopy (Karam et al. 1992, Ferrazoli et al. 2000) and snow (Fung 1994). Truck-mounted radiometers (Matzler 1990) and airborne instruments (Calvet et al. 1996, Wigneron et al. 1997, Hewison and English 1999, Hewison 2001) provide some in situ estimates of the emissivities to help anchor the models. However, even assuming that a perfect land surface emissivity model exists, would the inputs it will require (soil texture and humidity, vegetation characteristics, percentage of vegetation coverage within a field of view, snow density, to name only a few) be available on a global basis with a resolution compatible with the satellite resolution and with the required accuracy?

Very few groups have so far examined the problem of global microwave land surface emissivities as a first step for data assimilation over the continents.

Global land surface emissivity maps were first produced at Special Sensor Microwave/Imager (SSM/I) frequencies by Prigent et al. (1997, 1998), by removing the contribution of the atmosphere, clouds, and rain using ancillary data. The emissivities are estimated for SSM/I observation conditions, i.e., for a 53° zenith angle at 19.35, 22.235, 37.0 and 85.5 GHz. These emissivities have been the basis for a large number of studies, first to analyze the land surface characteristics like vegetation (Prigent et al. 2001 a) or inundation (Prigent et al. 2001 b, Filly et al. 2003), or to help retrieve surface skin temperature and atmospheric parameter over land (Prigent et al. 1999, Aires et al. 2001, Prigent et al. 2003). Frequency and angular intra-extrapolations of these SSM/I emissivities for SSM/T-1 and

AMSU-A application have been suggested (Prigent et al. 2000) but has not been used so far in an operational context. Similar direct calculations of the emissivities have also been performed by Felde and Pickle (1995) and Jones and Vonder Haar (1997), for limited geographical regions.

Differently, Weng et al. (2001) chose to develop a global model to estimate the emissivity for the various surface conditions encountered over the continents, using different radiative transfer solutions depending on the surface characteristics. Model inputs are provided by a land surface model, such as the one in the Global Data Assimilation System of the National Center for Environmental Prediction (NCEP). The simulations have been compared with both ground-based measurements and with emissivities directly calculated from AMSU-A observations.

As described by Kelly and Bauer (2000), the current forecast system at the European Centre for Medium-Range Weather Forecasts (ECMWF) uses an intermediate approach to assimilate 10 of the AMSU-A channels, two of which have a weak contribution from the surface (at 53.596 and 54.4 GHz). In this approach, the land surface emissivity is obtained from the observations by a parametric model after identification of the scene (Grody 1988). Despite the positive impact of the two AMSU-A surface-affected channels on the forecast quality (Kelly and Bauer 2000), the treatment of the surface emissivity is too simple to allow the extension of the approach to channels that are more affected by the surface, like at 52.8 GHz.

This study describes the work performed at ECMWF to apply the Prigent et al. (1997, 1998) approach to estimate the microwave land surface emissivities, within the specific context and constraint of operational assimilation.

This paper is organized as follows. The method used at ECMWF to directly calculate the land surface emissivities for AMSU-A observation is described (section 2). The results are then analyzed, with special emphasis on the evaluation of the frequency and angular dependencies of the emissivities with respect to the surface characteristics. Possible extrapolation of the SSM/I emissivities to the AMSU ones is considered. Direct calculation results are also compared with emissivity model outputs. The last section concludes on the method that is selected.

2. Direct calculation of the land surface emissivities for the AMSU-A frequencies and observation conditions

The method adopted to directly calculate the land surface emissivities at AMSU-A frequencies and observation conditions follows closely the scheme previously developed for SSM/I (Prigent et al. 1997, 1998). It uses 1) the AMSU-A observed brightness temperatures, 2) the Radiative Transfer for

Tiros Operational Vertical Sounder (RTTOV) (Eyre 1991, Saunders et al. 1999) atmospheric radiation model, 3) the ECMWF short-range forecasts.

2.1. The method

2.1.1. Basic principal. Over a flat lossy surface, the integrated radiative transfer equation in the Rayleigh-Jeans approximation, for a non scattering plane-parallel atmosphere can be expressed in terms of brightness temperature for a given polarization state p :

$$Tb_p = T_{surf} \times \epsilon_p \times e^{-\tau(0,H)/\mu} + T_{atm}^\downarrow \times (1 - \epsilon_p) \times e^{-\tau(0,H)/\mu} + T_{atm}^\uparrow \quad (1)$$

with $T_{atm}^\downarrow = \int_H^0 T(z) \alpha(z) e^{-\tau(z,0)/\mu} dz$ and $T_{atm}^\uparrow = \int_0^H T(z) \alpha(z) e^{-\tau(z,H)/\mu} dz$. Tb_p is the brightness temperature measured by the satellite for polarization state p ; T_{surf} is the surface "skin" temperature; ϵ_p is the surface emissivity for polarization state p ; $\mu = \cos(\theta)$, θ being the incidence angle on the surface; $\alpha(z)$ is the atmospheric absorption by gases at altitude z ; $T(z)$ is the atmospheric temperature at altitude z ; $\tau(z_0, z_1) = \int_{z_0}^{z_1} \alpha(z) dz$ is the atmospheric extinction from z_0 to z_1 ; and H is the orbiter height.

This equation leads to:

$$\epsilon_p = \frac{Tb_p - T_{atm}^\uparrow - T_{atm}^\downarrow \times e^{-\tau(0,H)/\mu}}{e^{-\tau(0,H)/\mu} \times (T_{surf} - T_{atm}^\downarrow)} \quad (2)$$

At AMSU-A frequencies, the radiation emanates from only a thin surface layer of bare soil and water with the penetration depth of the order of the wavelength in soil and less for water. That leads to the following assumptions: there is no volume scattering, the surface temperature is the skin temperature, and for flat surfaces the reflection is considered specular. However, volume scattering is involved in the cases of vegetation, snow cover, or very dry sand since the microwave radiation can arise from below and within the canopy or snow layer. When the terrain is rough on scales between the radiation wavelength and the size of the field of view, the surface acts as a set of scattering facets with a complex distribution of orientations. In these cases (1) and (2) involve some "effective" emissivity and temperature, aggregated over the depth of penetration and the field of view of the satellite instrument (English and Hewison 1998, Deblonde 2000).

For simplicity sake in the following, the term surface emissivity will be used instead of "effective" surface emissivity.

The method consists in solving the radiative transfer equation (2) for the surface emissivity for each channel using ancillary data to specify the atmospheric and other surface parameters.

2.1.2. Validity of the specular approximation. The validity of the specular approximation has been evaluated by comparing the difference between obtained emissivities using the specular approach and emissivities calculated assuming a pseudo-Lambertian surface (Figure 1). For the pseudo-Lambertian case, the downwelling radiations come from a cone centered on the specular angle with a 10° Gaussian distribution. The simulations have been conducted for specular emissivities from 0.7 to 1, and for observation angles up to 60° . Results are shown for a US standard atmosphere (integrated water vapor content 14 kg/m^2). For this atmosphere at nadir the atmospheric transmission is 0.92, 0.95, 0.69, and 0.83 at 23, 31, 50, and 89 GHz respectively. The obtained emissivity differences are small. Even for high observation angles the errors related to the specular approximation are within 1% for all channels.

2.1.3. Application to AMSU-A data at ECMWF. The AMSU-A emissivity calculations are performed using the ancillary data provided by the ECMWF short-range (0-12 hours) forecasts, at same location and time than the satellite observations. In a first step, cloudy observations are eliminated. Compared to what has been done for SSM/I previously (Prigent et al. 1997, 1998), the main difference arises from the fact that the cloud, surface skin and atmospheric products are not derived from the International Satellite Cloud Climatology Project (ISCCP) (Rossow and Schiffer 1999). The ISCCP data are not available in real time which prevents their use in NWP operational assimilation schemes. Here the selection of the clear pixels is based on the forecast model, i.e. the observations that correspond to a non-zero fractional area cloud cover in the model are excluded. The atmospheric contribution is then calculated from the forecast model variables and the RTTOV radiative transfer model. Finally, with the forecast model surface temperature, the “effective” surface emissivity is calculated from (2).

Whatever the ancillary information source is, its errors affect the emissivity retrieval. Prigent et al. (1997) discuss the emissivity errors when using the ISCCP data and conclude in favor of a 1% accuracy for the retrieved emissivities. When using ECMWF data, the error caused by the atmospheric products is limited, since the ECMWF analysis interpolated to +/- 30 minutes from the satellite observations are used. This is not the case for the error coming from the cloud and surface skin temperature products since no such observations are yet assimilated at ECMWF: these variables are indirectly constrained by other observation types (like wind sensors for clouds). Still, the skin temperature error lies within the 4 K figure used in the Prigent et al. (1997) study, except in very dry regions (Trigo and Viterbo 2003).

Also, cloud occurrence in the ECMWF short-range forecast is realistic if we except convection regions (Chevallier and Kelly 2002). In summary, the 1% accuracy previously quoted is expected to apply to the present computations, except in some regions like deserts and the inter-tropical convergence zone, where biases are likely to occur

2.2. Brief description of the AMSU-A instrument

The AMSU-A instruments is described in Diak et al. (1992) and Saunders et al. (1993). It is a cross-track scanning instrument, with 30 scan positions at 3.3° intervals from $-14.5 \times 3.3^\circ$ to $+14.5 \times 3.3^\circ$ which translate into local zenith angles θ_z up to 58.5° . The spatial resolution is of 50 km at nadir. Table 1 summarizes the AMSU-A characteristics and gives the total atmospheric transmission at nadir for each channel for two standard atmospheres. The polarization measured by AMSU-A rotates with scan angle due to the rotating-reflector/fixed-feed type of antenna design. If θ_s is the scan angle and θ_z is the local zenith angle, then the AMSU-A surface emissivity $\epsilon(\theta_z)$ seen for a local zenith angle θ_z is given by:

$$\epsilon(\theta_z) = \epsilon_p(\theta_z) \cos^2(\theta_s) + \epsilon_q(\theta_z) \sin^2(\theta_s) \quad (3)$$

$\epsilon_p(\theta_z)$ and $\epsilon_q(\theta_z)$ are the two orthogonal polarized surface emissivities at θ_z local zenith angle. Depending on the channels, p will represent the vertical or the horizontal polarization. The polarization p seen when the incidence is close to nadir (i. e. for $\theta_z=\theta_s$ very close to 0°) is indicated for each channel on Table 1.

2.3. Emissivity maps

Calculations are performed globally for two months: July 2002 and January 2003, with data from NOAA-15, NOAA-16, and NOAA-17. They have been mapped to the forecast model regular 40 km grid (T511 spectral truncature).

Figure 2 shows the average number of AMSU-A observations per grid cell, for two incidence angle ranges (10° - 20° and 40° - 50°), for clear and cloudy scenes together (x) and for cloud-free observations only (o). Results are presented for July 2002. For other months, the amount of cloud cover changes with latitude, but still the number of observations per grid cell and per incidence angle is small (less than 4). We checked that the results presented in the following are not significantly affected by relaxing the cloud detection, i.e. letting observations with up to 5% model low and medium cloud cover and allowing any amount of model high clouds.

Figure 3 shows the mean emissivities for 4 frequencies, for two incidence angle ranges (10° - 20° on

the left and 40° - 50° on the right). For the channels with atmospheric transmission lower than $\sim 20\%$ at nadir, the emissivity estimates are very noisy (not shown): the surface contribution to the observed signal is limited and errors in the radiative transfer model or in the atmospheric profiles have a larger impact on the emissivity calculation. The expected spectral variation of the emissivities being limited, extrapolations of the emissivities to the other channels in the O₂ band will be valid. The calculated emissivities show consistent spatial structures, that can be related to the surface characteristics. Holes in the map are due to the lack of clear sky observations for this month for the observations with the given incidence angle range (the tropical band is particularly affected). As predicted by the models, the emissivities are higher in vegetated areas (e.g., the Siberian forest) than in arid region (e.g., the North African deserts and the Arabic Peninsula). Low emissivities are associated with areas of standing water or of highly saturated soils (North of Canada, areas around the river Ob in Siberia or the Parana river in South America). Frequency and angular variations seem limited (the maps are rather similar), except for the 50.3 GHz map for high incidence angle. Further analysis of these frequency and angular variations is performed in the next section.

3. Analysis and evaluation of the emissivity calculations. Comparison with other emissivity estimates

Because of the lack of direct information about the surface emissivity at these relatively large spatial scales, one can only check that the expected behaviors are found. Evaluation strategy will be twofold: (1) to carefully check the consistency of the retrieved AMSU-A emissivities among themselves by verifying their frequency and angular dependencies, (2) to compare them with other microwave emissivities estimated at global scale.

For comparison purposes, two other emissivity calculations have been performed at ECMWF for the same two months. First, the SSM/I emissivities have been calculated, using the same radiative transfer code and the same ECMWF input data. SSM/I being a conical scanner, the incidence angle is fixed and each scene is observed more often under the same observing conditions (see Figure 2 in Prigent et al (1997)), reducing the noise in monthly mean estimates of the surface emissivity for a given location. Assuming that the frequency and angular dependencies of the emissivities are well known, estimates of the AMSU-A emissivities could be derived from the SSM/I emissivities. The frequency and angular intra-extrapolation schemes previously developed (Prigent et al. 2000) will be tested here. Second, the Weng et al. (2001) emissivity model has also been implemented at ECMWF.

The vegetation classification from Matthews (1983) is selected to sort the data by vegetation types.

It is compiled from a large number of published sources and is independent of the data sets used here. The vegetation data distinguishes 30 classes, which are further grouped.

The angular dependence of the AMSU-A emissivities directly calculated (section 2) is first analyzed. For four surface types, Figure 4 shows the mean emissivities and their standard deviation, for the four AMSU-A window channel frequencies for six ranges of incidence angles for January 2003. For each angular range, the monthly mean emissivity values are presented, along with their standard deviations over the month. The emissivities do not vary significantly with incidence angle up to $\sim 40^\circ$, and then they decrease with increasing angle. Given the polarization features of the AMSU-A observations, this is fully compatible with model simulations. On the same figure, comparison is provided with the angular and frequency fits derived from the corresponding SSM/I emissivity calculation performed at ECMWF for the same month (the middle solid line indicates the mean with the two others giving the standard deviation). The emissivity angular fit (Prigent et al. 2000) was derived from simulations for various surface types with the RADTRAN model (Isaacs et al. 1989). The figure clearly shows that the expected angular behavior is obtained, except for the 50.3 GHz channel for large angles. Over snow, the emissivities are more variable (larger standard deviations). They are sensitive to snow physical properties: interaction of the microwave radiation with snow involves volume scattering, especially for dry snow at high frequency (Matzler 1994). Similar behaviors are observed in July (not shown).

Figure 5 presents the frequency dependence of the AMSU-A directly calculated emissivities for the four window channels and for four surface types, as calculated for July 2002, along with their standard deviations over the month. Only data for NOAA-16 with viewing angles smaller than 40 degrees are shown. The distinction is made between local night-time and day-time observations, since the NOAA-16 spacecraft crosses the equator at about 1:30 AM/PM LST. For comparison, the platforms that carry the SSM/I instruments cross the equator between 5:30 and 9:30 AM/PM LST.

As expected, for snow-free surface types, the frequency dependence of the emissivities as derived from the AMSU estimates is rather limited, with the emissivities slightly decreasing with increasing frequencies. This is very important: it means that interpolation/extrapolation of the emissivity calculation from the AMSU window channels to the AMSU sounding ones is possible. The frequency dependence estimated from the SSM/I derived emissivities (as extrapolated in angle and frequencies to AMSU conditions) is more pronounced. However, one will note that the agreement between the SSM/I extrapolated values and the AMSU 50.3 GHz is especially good for this broad angular range, whatever the surface. This is very encouraging for the extrapolation to the emissivities for the 50-60 GHz O₂ channels. Comparison of the night and day time NOAA-16 emissivity estimate shows a rather similar

frequency behavior, except over desert surfaces. The lower the frequency, the larger the difference between the night and day time estimates, with a mean difference of ~ 0.02 at 23.8 GHz. This can be explained by different penetration depth of the radiation in dry sand desert. In our calculation (equ. 1), the radiation is expected to emerge from a very thin surface layer that radiates according to the physical temperature of a thin layer at the surface (the skin temperature). However, in dry sand deserts, the microwave radiation might come from below the surface, the lower the frequency, the larger the penetration depth. Sand desert having a limited thermal inertia, strong thermal vertical gradients are observed below the surface, along with large diurnal cycle. As a consequence, the 'effective' emissivities that are calculated with the skin temperature vary during the diurnal cycle. This phenomenon had been analyzed in details at SSM/I frequencies (Prigent et al. 1999). In addition, residual differences between the night and day time estimates for frequencies and regions where penetration of the radiation is not expected (at 89 GHz over grassland for instance) can also be related to an inadequate modeling of the surface skin temperature diurnal cycle in the ECMWF forecast model (Trigo and Viterbo 2003).

Differences between the AMSU-A directly calculated emissivities and the emissivities derived from SSM/I calculations are quantified in Table 2. Results include July and January values for the four window channels and for 2 incidence angle ranges, separated per vegetation types. Mean differences are indicated along with the r.m.s. difference (in parenthesis). Biases are $\sim 1\%$ or below for all surface types, even for snow, with r.m.s. values ~ 0.02 (slightly larger for snow). The behavior of the 50.3 GHz channel for large angles is still the exception.

Monthly mean emissivity atlases have been calculated at NASA/Goddard Institute for Space Studies for the SSM/I frequencies and observations conditions for several years. From a practical point of view, it would be convenient to be able to inter-extrapolate these emissivities to the AMSU-A conditions, using the frequency and angular fit developed (Prigent et al. 2000). Direct calculations from AMSU-A have been compared to the inter-extrapolated SSM/I emissivities previously calculated at NASA/GISS for July 1992 and January 1993. The results are presented on Table 3. Although the SSM/I emissivities were calculated using different inputs (NCEP reanalysis (Kalnay et al. 1996) and ISCCP data) and a different radiative transfer code, although inter-annual variability of the surface characteristics influences the emissivities, the overall results are very similar to the results given in Table 2. Not surprisingly, the r.m.s. errors are slightly larger, especially for the snow that can show rather large inter-annual variability in extent and in physical properties. This is clearly seen at 89 GHz which is particularly sensitive to snow properties.

Finally, the AMSU-A directly calculated emissivities are compared to the simulations of the Weng

et al. (2001) emissivity model using the forecast model relevant surface variables (soil temperature and humidity, vegetation fraction, and snow depth) in input. The results are presented on Table 4. The agreement with the SSM/I-based estimation is less good than for the previous results in Tables 2 and 3, likely because of both the simplicity of the ECMWF land surface model and that of the emissivity model. This is particularly true for desert and snow surfaces where most biases are larger than 1%. Weng et al. (2001) already noticed the limitations of the snow emissivity model.

4. Discussion and Conclusion

Over land surfaces, the utilization of passive microwave observations is usually limited to middle and upper tropospheric sounding channels due to the lack of good surface emission modeling. At ECMWF, AMSU-A data that is affected by the surface (channels 5 and 6 at 53.6 ± 0.115 and 54.4 GHz) is therefore assimilated rather conservatively assuming constant surface emissivities associated with several coarsely defined surface types. The surface type classification employs AMSU-A window channels at 23.8, 31.4, 50.3 and 89.0 GHz and does not take into account the variation of emissivity with scan angle.

In this paper, a new approach for extending the data usage over land was presented that provides a more dynamical emissivity estimate as a function of the local states of atmosphere and surface, respectively. Surface emissivity is derived using the ECMWF background information on surface skin temperature as well as atmospheric temperature and moisture profiles with observations at those frequencies that are not used in the assimilation. Two options are identified in which (1) the inversion is carried out at only one frequency (50.3 GHz) assuming that the emissivity is identical to that at 52.8, 53.6 ± 0.115 and 54.4 GHz; (2) emissivities are derived separately at 23.8, 31.4 and 89.0 GHz and linearly interpolated to the frequency of choice. The advantage of the second option is the much smaller atmospheric opacity in the window channels. This is rather important because errors in the background information may alias the surface emissivity estimate and therefore negatively impact the analysis. However, the interpolation over frequencies and the difference in polarization variation across the scan between window and sounding channels introduce uncertainties as well.

Surface emissivities have been calculated at 23.8, 31.4, 50.3 and 89.0 GHz for two months and compared to other satellite products due to the lack of independent validation data. It was found that both the angular variation and frequency dependence of emissivity were rather small for zenith angles below 40 degrees and over all surface types except snow covered regions. Also, surfaces that show distinct volume scattering (dry soil and sand) exhibited a larger dispersion in the comparison as a

function of daytime.

Differences between the two products were found to be rather small and mainly associated with the above mentioned scattering surface types, i.e., sand and snow, and scan position (at 50.3 GHz only). Another possibility of evaluation was exploited that is the forward calculation of emissivity using physical surface and vegetation parameters available from the ECMWF model parameterizations such as soil type, soil moisture, vegetation coverage and water content. In this case, the derived and modeled emissivities showed larger discrepancies that can be interpreted as shortcomings in emissivity modeling and the limited accuracy of the input parameters.

The final means of evaluation is the test of the scheme in the ECMWF data assimilation context. For this purpose, two experiments were carried, namely a control experiment with the operational configuration and an experiment that employed the derivation of emissivity at the window frequencies with interpolation to the sounding frequencies. Two model cycles were performed on July 18, 2003, at 00 and 12 UTC. In the control experiment, AMSU-A channel 4 (52.8 GHz), was not used in the assimilation but for data screening. In the emissivity experiment, this channel was activated as well.

Over land, a total number of 410309 AMSU-A observations were counted of which 0, 18602 and 23634 were used in the minimization of the control experiment for channels 4, 5 and 6, respectively. In the emissivity experiment these numbers increased to 26383, 22174, 27712, that is an increase by 17-19 % in channels 5 and 6 because more data passed the quality control (which is based on observations minus calculations). This increase of observation numbers is quite significant, however, the impact on the forecast was small and overall neutral. It has to be noted that data screening and observation error quantification treatment remained unchanged. In the future, these would have to be revised for an optimum utilization of the information contained in the additional observations that are sensitive to the lower troposphere over land.

Acknowledgments. We wish to thank Jean-Noel Thépaut (ECMWF) for his support and for his careful review of an earlier version of the paper. We are very grateful to Stephen English and two other anonymous reviewers for detailed and constructive comments on the manuscript. Part of this work was done in the context of the Satellite Application Facility on Numerical Weather Prediction which is co-sponsored by EUMETSAT.

References

- Aires, F., C. Prigent, W. B. Rossow, and M. Rothstein, 2001: A new neural network approach including first-guess for retrieval of atmospheric water vapor, cloud liquid water path, surface temperature and emissivities over land from satellite microwave observations. *J. Geophys. Res.*, **106**, 14 887-14 907.
- Calvet, J.-C., A. Chanzy, and J.-P. Wigneron, 1996: Surface temperature and soil moisture retrieval in the Sahel from airborne multifrequency microwave radiometry. *IEEE Trans. Geosc. Remote Sensing*, **34**, 588-600.
- Chevallier, F., and G. Kelly, 2002: Model clouds as seen from space: comparison with geostationary imagery in the 11 μ m window channel. *Mon. Wea. Rev.*, **130**, 712-722.
- Deblonde, G., 2000: Evaluation of FASTEM and FASTEM2. NWP SAF report, The Met Office, Exeter, UK, 33 pp.
- Diak, G. R., D. Kim, M. S. Whipple, and X. Wu, 1992: Preparing for the AMSU. *Bull. Am. Meteorol. Soc.*, **73**, 1971-1984.
- English, S. J., 2000: Estimation of temperature and humidity profile information from microwave radiances over different surface types. *Journ. Applied Meteorology*, **38**, 1526-1541.
- English, S. J., R. J. Renshaw, P. C. Dibben, A. J. Smith, P. J. Rayer, C. Poulsen, F. W. Saunders, and J. R. Eyre, 2000: A comparison of the impact of TOVS and ATOVS satellite sounding data on the accuracy of numerical weather forecasts. *Q. J. R. Meteorol. Soc.*, **126**, 2911-2931.
- English, S. J., and T. Hewison, 1998: A fast generic millimeter-wave emissivity model. Proceedings of SPIE, 3503, 288-300.
- Eyre, J. R., 1991: A fast radiative transfer model for satellite sounding systems. *ECMWF Technical Memorandum No. 176*, 28 pp.
- Felde, G. W. and J. D. Pickle, 1995: Retrieval of 91 and 150 GHz Earth surface emissivities. *J. Geophys. Res.*, **100**, 20855-20866.
- Ferrazoli, P., J.-P. Wigneron, L. Guerriero, and A. Chanzi, 2000: Multifrequency emission of wheat: Modeling and applications. *IEEE Trans. Geosc. Remote Sensing*, **38**, 2598-2607.
- Filly, M., A. Royer, K. Goita, and C. Prigent, 2003: A simple retrieval method for land surface temperature and fraction of water surface determination from satellite microwave brightness temperatures in sub-arctic areas, *Remote Sens. Environ.*, **85**, 328-338.
- Fung, A. K., 1994: Microwave scattering and emission models and their applications. Norwood, MA, Artech House.
- Grody, N. C., 1988: Surface identification using satellite microwave radiometers. *IEEE Trans. Geosci. Remote Sens.*, **26**, 850-859.
- Hewison, T. J. and S. J. English, 1999: Airborne retrievals of snow and ice surface emissivity at millimeter wavelength. *IEEE Trans. Geosc. Remote Sensing*, **37**, 1871-1879.
- Hewison, T. J., 2001: Airborne measurements of forest and agricultural land surface emissivity at millimeter

- wavelengths. *IEEE Trans. Geosc. Remote Sensing*, **39**, 393-400.
- Isaacs, R. G., Y.-Q. Jin, R. D. Worsham, G. Deblonde, and V. J. Falcone, 1989: The RADTRAN microwave surface emission models. *IEEE Trans. Geosc. Remote Sensing*, **27**, 433-440.
- Jones, A. S., and T. H. Vonder Haar, 1997: Retrieval of surface emittance over land using coincident microwave and infrared satellite measurements. *J. Geophys. Res.*, **102**, 13609-13626.
- Kalnay, E. et al., 1996: The NCEP/NCAR 40-year reanalysis project. *Bull. Am. Meteorol. Soc.*, **77**, 437-470.
- Karam, M. A., A. K. Fung, R. H. Lang, and N. S. Chuahan, 1992: A microwave scattering model for layered vegetation. *IEEE Trans. Geosc. Remote Sensing*, **30**, 767-784.
- Kelly, G., and P. Bauer, 2000: The use of AMSU-A surface channels to obtain surface emissivity over land, snow and ice for Numerical Weather Prediction. *Proc. of the Eleventh International TOVS Study Conference, Budapest, Hungary*, 167-179.
- Matthews, E., 1983: Global vegetation and land use: new high-resolution data bases for climate studies. *J. Clim. Appl. Meteorol.*, **22**, 474-486.
- Matzler, C., 1990: Seasonal evolution of microwave radiation from an oat field. *Remote Sens. Environ.*, **31**, 161-173.
- Matzler, C., 1994: Passive microwave signatures of landscapes in winter. *Meteorology and Atmospheric Physics*, **54**, 241-260.
- Prigent C., W. B. Rossow, and E. Matthews, 1997: Microwave land surface emissivities estimated from SSM/I observations. *J. Geophys. Res.*, **102**, 21867-21890.
- Prigent, C., W. B. Rossow, and E. Matthews, 1998: Global maps of microwave land surface emissivities: Potential for land surface characterization. *Radio Sci.*, **33**, 745-751.
- Prigent, C., W. B. Rossow, and E. Matthews, 1999: Microwave radiometric signatures over different surface types in deserts. *J. Geophys. Res.*, **104**, 12147-12158.
- Prigent, C., J. P. Wigneron, W. B. Rossow, and J. R. Pardo-Carrion, 2000: Frequency and angular variations of land surface microwave emissivities: Can we estimate SSM/T and AMSU emissivities from SSM/I emissivities?. *IEEE Trans. Geosc. Remote Sensing*, **38**, 2373-2386.
- Prigent, C., F. Aires, W. B. Rossow, and E. Matthews, 2001 a: Joint characterization of vegetation by satellite observations from visible to microwave wavelength: A sensitivity analysis. *J. Geophys. Res.*, **106**, 20665-20685.
- Prigent, C., E. Matthews, F. Aires, and W. B. Rossow, 2001 b: Remote sensing of global wetland dynamics with multiple satellite data sets. *Geophys. Res. Lett.*, **28**, 4631-4634.
- Prigent, C., F. Aires, and W. B. Rossow, 2003: Land surface skin temperatures from a combined analysis of microwave and infrared satellite observations for an all-weather evaluation of the differences between air and skin temperatures. *J. Geophys. Res.*, **108**, 4310-4321.
- Rossow, W. B., and R. A. Schiffer, 1999: Advances in understanding clouds from ISCCP. *Bull. Am. Meteorol.*

- Soc.*, **80**, 2261-2287.
- Saunders, R. W., 1993: Note on the Advanced Microwave Sounding Unit. *Bull. Am. Meteorol. Soc.*, **74**, 2211-2212.
- Saunders, R., M. Matricardi, and P. Brunel, 1999: An improved fast radiative transfer model for assimilation of satellite radiance observations. *Quart. J. Roy. Meteor. Soc.*, **125**, 1407-1425.
- Shi, J., K. S. Chen, Q. Li, T. J. Jackson, and P. E. O'Neil, 2002: A parameterized surface reflectivity model and estimation of bare-surface soil moisture with L-band radiometer. *IEEE Trans. Geosc. Remote Sensing*, **40**, 2674-2686.
- Trigo, I. F., and P. Viterbo, 2003: A comparison between observations and the ECMWF model. *J. Appl. Meteor.*, **42**, 1463-1479.
- Weng, F., B. Yan, and N. C. Grody, 2001: A microwave land emissivity model. *J. Geophys. Res.*, **106**, 20115-20123.
- Wigneron, J.-P., D. Guyon, J.-C. Calvet, G. Courrier, and N. Bruguier, 1997: Monitoring coniferous forest characteristics using a multifrequency (5-90 GHz) microwave radiometer. *Remote Sens. Environ.*, **60**, 299-310.

Received _____

Table1. AMSU-A characteristics

Table2. Difference between AMSU-A emissivities directly calculated and emissivities estimated from intra-extrapolations of the SSM/I emissivities calculated at ECMWF for the same months and years. Biases are indicated, along with r.m.s. values (in parenthesis).

Table3. Difference between AMSU-A emissivities directly calculated and emissivities estimated from intra-extrapolations of the SSM/I emissivities previously calculated at NASA/GISS for the same months but different years. Biases are indicated, along with r.m.s. values (in parenthesis).

Table4. Difference between AMSU-A emissivities directly calculated and emissivities simulated with Weng et al. (2001) model. Biases are indicated, along with r.m.s. values (in parenthesis).

Table 1. AMSU-A characteristics

Channel number	Frequency (GHz)	Polarization at nadir	Atmospheric transmission (tropical)	Atmospheric transmission (winter subarctic)
1	23.8	V	.78	.99
2	31.4	V	.89	.96
3	50.3	V	.63	.68
4	52.8	V	.29	.32
5	53.596±.115	H	.11	.13
6	54.40	H	.02	.02
7	54.94	V	.00	.00
8	55.50	H	.00	.00
9	57.290=ν	H	.00	.00
10	ν±.217	H	.00	.00
11	ν ± .322 ± .048	H	.00	.00
12	ν ± .322 ± .022	H	.00	.00
13	ν ± .322 ± .010	H	.00	.00
14	ν ± .322 ± .0045	H	.00	.00
15	89.0	V	.61	.91

Table 2. Difference between AMSU-A emissivities directly calculated and emissivities estimated from intra-extrapolations of the SSM/I emissivities calculated at ECMWF for the same months and years. Biases are indicated, along with r.m.s. values (in parenthesis).

		Forest	Grassland	Desert	Snow	TOTAL
Frequency	Angle					
23.80 GHz	15°	-.003 (.014)	.000 (.012)	-.001 (.012)	-.011 (.029)	-.004 (.019)
	45°	-.011 (.021)	.008 (.017)	-.011 (.018)	-.005 (.018)	-.009 (.019)
31.42 GHz	15°	-.002 (.014)	.000 (.012)	-.002 (.012)	-.007 (.027)	-.002 (.018)
	45°	-.009 (.021)	-.006 (.017)	-.009 (.017)	-.004 (.020)	-.007 (.018)
50.33 GHz	15°	-.002 (.022)	.006 (.020)	-.003 (.017)	.000 (.028)	.003 (.022)

Table 2. (continued)

		Forest	Grassland	Desert	Snow	TOTAL
Frequency	Angle					
89.00 GHz	45°	-.036 (.063)	-.027 (.051)	-.031 (.044)	-.060 (.098)	-.040 (.066)
	15°	.013 (.023)	.014 (.024)	.006 (.017)	.004 (.032)	.009 (.025)
	45°	.004 (.024)	.007 (.023)	-.001 (.018)	.004 (.032)	.004 (.025)

Table 3. Difference between AMSU-A emissivities directly calculated and emissivities estimated from intra-extrapolations of the SSM/I emissivities previously calculated at NASA/GISS for the same months but different years. Biases are indicated, along with r.m.s. values (in parenthesis).

Frequency	Angle	Forest	Grassland	Desert	Snow	TOTAL
23.80 GHz	15°	-.002 (.022)	.001 (.023)	-.001 (.016)	-.012 (.041)	-.003 (.028)
	45°	-.011 (.027)	-.005 (.024)	-.008 (.019)	-.010 (.034)	-.008 (.026)
31.42 GHz	15°	.000 (.022)	.004 (.023)	.002 (.015)	-.009 (.040)	-.001 (.028)
	45°	-.009 (.026)	-.001 (.024)	-.006 (.018)	-.009 (.038)	-.006 (.028)
50.33 GHz	15°	.000 (.028)	.007 (.033)	.003 (.021)	-.005 (.046)	.001 (.035)
	45°	-.042 (.073)	-.025 (.055)	-.026 (.042)	-.070 (.117)	-.041 (.079)
89.00 GHz	15°	-.002 (.025)	.006 (.038)	-.004 (.022)	.013 (.065)	.003 (.045)
	45°	-.012 (.032)	.000 (.042)	-.009 (.025)	-.014 (.070)	-.008 (.049)

Table 4. Difference between AMSU-A emissivities directly calculated and emissivities simulated with Weng et al. (2001) model. Biases are indicated, along with r.m.s. values (in parenthesis).

Frequency	Angle	Forest	Grassland	Desert	Snow	TOTAL
23.80 GHz	15°	.015 (.038)	.008 (.033)	-.004 (.025)	-.099 (.140)	-.023 (.077)
	45°	.008 (.044)	.000 (.037)	-.014 (.033)	-.053 (.091)	-.015 (.055)
31.42 GHz	15°	.006 (.034)	.000 (.031)	-.009 (.026)	-.070 (.103)	-.021 (.059)
	45°	.000 (.041)	-.006 (.035)	-.017 (.034)	-.034 (.069)	-.015 (.046)

Table 4. (continued)

		Forest	Grassland	Desert	Snow	TOTAL
Frequency	Angle					
50.33 GHz	15°	-.009 (.043)	-.010 (.036)	-.011 (.031)	.131 (.162)	.027 (.089)
	45°	-.046 (.087)	-.044 (.073)	-.045 (.065)	.083 (.175)	-.014 (.107)
89.00 GHz	15°	-.018 (.039)	-.020 (.037)	.021 (.058)	.507 (.546)	.132 (.284)
	45°	-.025 (.032)	-.029 (.042)	-.016 (.025)	.463 (.521)	.101 (.258)

Figure 1. The difference between specular and pseudo-Lambertian calculations for four AMSU-A frequencies and for surface emissivities varying between 0.7 and 1. For the pseudo-Lambertian calculation, the downwelling radiation comes from a cone centered on the specular angle with a 10° Gaussian distribution, whereas in the specular approximation the calculation only considers the downwelling radiation in the specular direction.

Figure 2. The average number of AMSU-A observations per grid cell, for two incidence angle ranges (10° - 20° and 40° - 50°), for clear and cloudy scenes together (x) and for cloud-free observations only (o). Results are presented for July 2002.

Figure 3. Monthly mean emissivity maps for July 2002 for four AMSU-A channel frequencies for two incidence angle ranges (10° - 20° on the left and 40° - 50° on the right).

Figure 4. Angular dependence of the AMSU-A monthly mean emissivities, as directly calculated for January 2003, separated per surface types, for the four window channels. The standard deviations are indicated for each mean value (error bars). Comparison is provided with the angular and frequency fits derived from the corresponding SSM/I emissivity calculation performed at ECMWF for the same month (the middle solid line indicates the mean with the two others giving the standard deviation). The emissivity and the incidence angle labels are the same for all the boxes.

Figure 5. Frequency dependence of the NOAA-16 AMSU-A monthly mean emissivities, as directly calculated for July 2002, for incidence angles smaller than 40 degrees, separated per surface types. The standard deviations are indicated for each mean value (error bars). Comparison is provided with the angular and frequency fits derived from the corresponding SSM/I emissivity calculation performed at ECMWF for the same month (the middle solid line indicates the mean with the two others giving the standard deviation). The distinction is made between local night- and day-time observations. From top to bottom: grassland, forest, snow, and desert areas.

Figure 1. The difference between specular and pseudo-Lambertian calculations for four AMSU-A frequencies and for surface emissivities varying between 0.7 and 1. For the pseudo-Lambertian calculation, the downwelling radiation comes from a cone centered on the specular angle with a 10° Gaussian distribution, whereas in the specular approximation the calculation only considers the downwelling radiation in the specular direction.

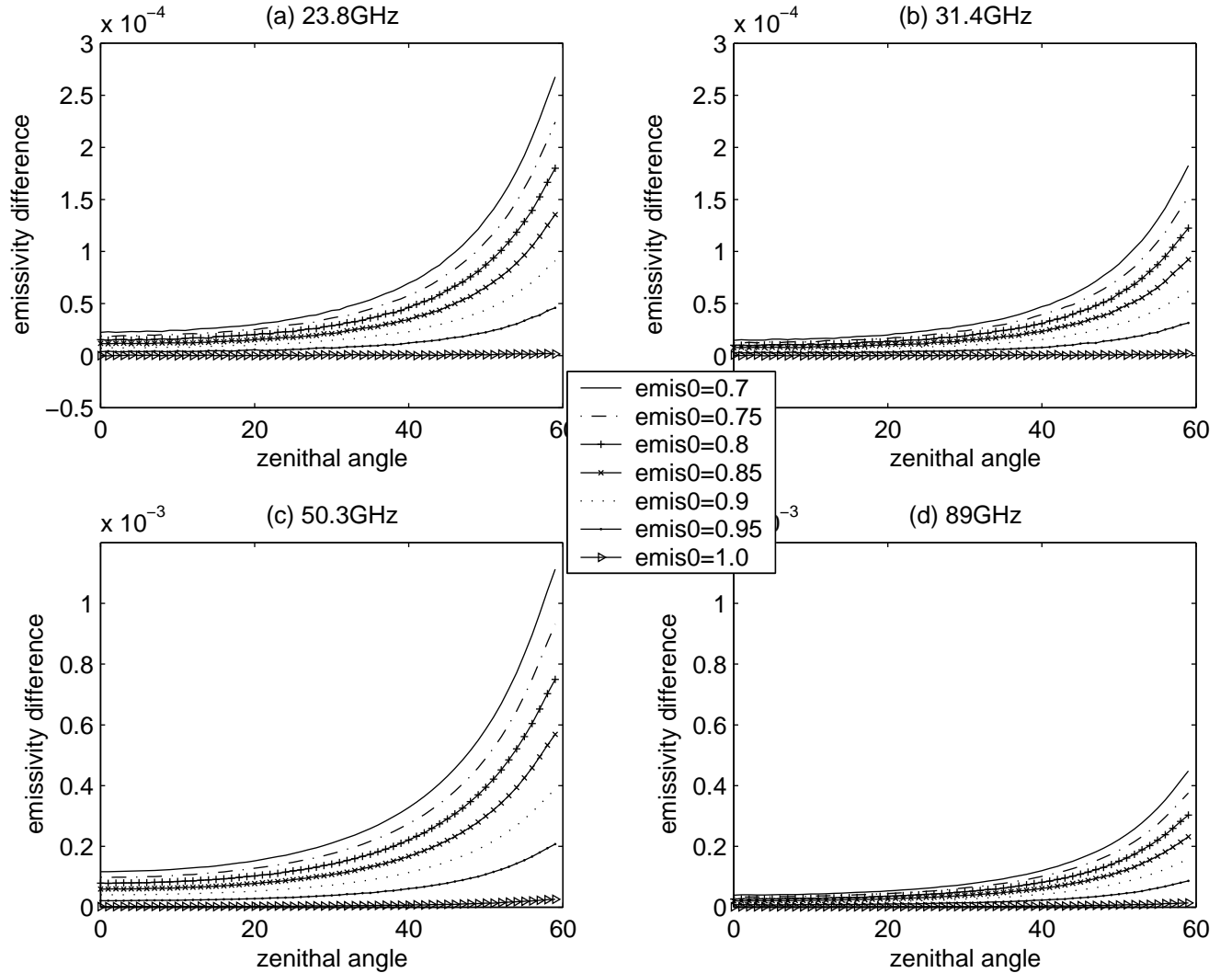


Figure 2. The average number of AMSU-A observations per grid cell, for two incidence angle ranges (10° - 20° and 40° - 50°), for clear and cloudy scenes together (x) and for cloud-free observations only (o). Results are presented for July 2002.

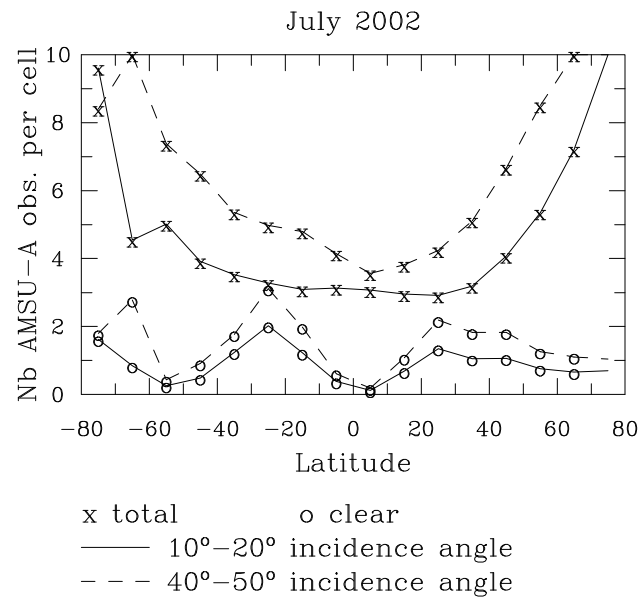


Figure 3. Monthly mean emissivity maps for July 2002 for four AMSU-A channel frequencies for two incidence angle ranges (10° - 20° on the left and 40° - 50° on the right).

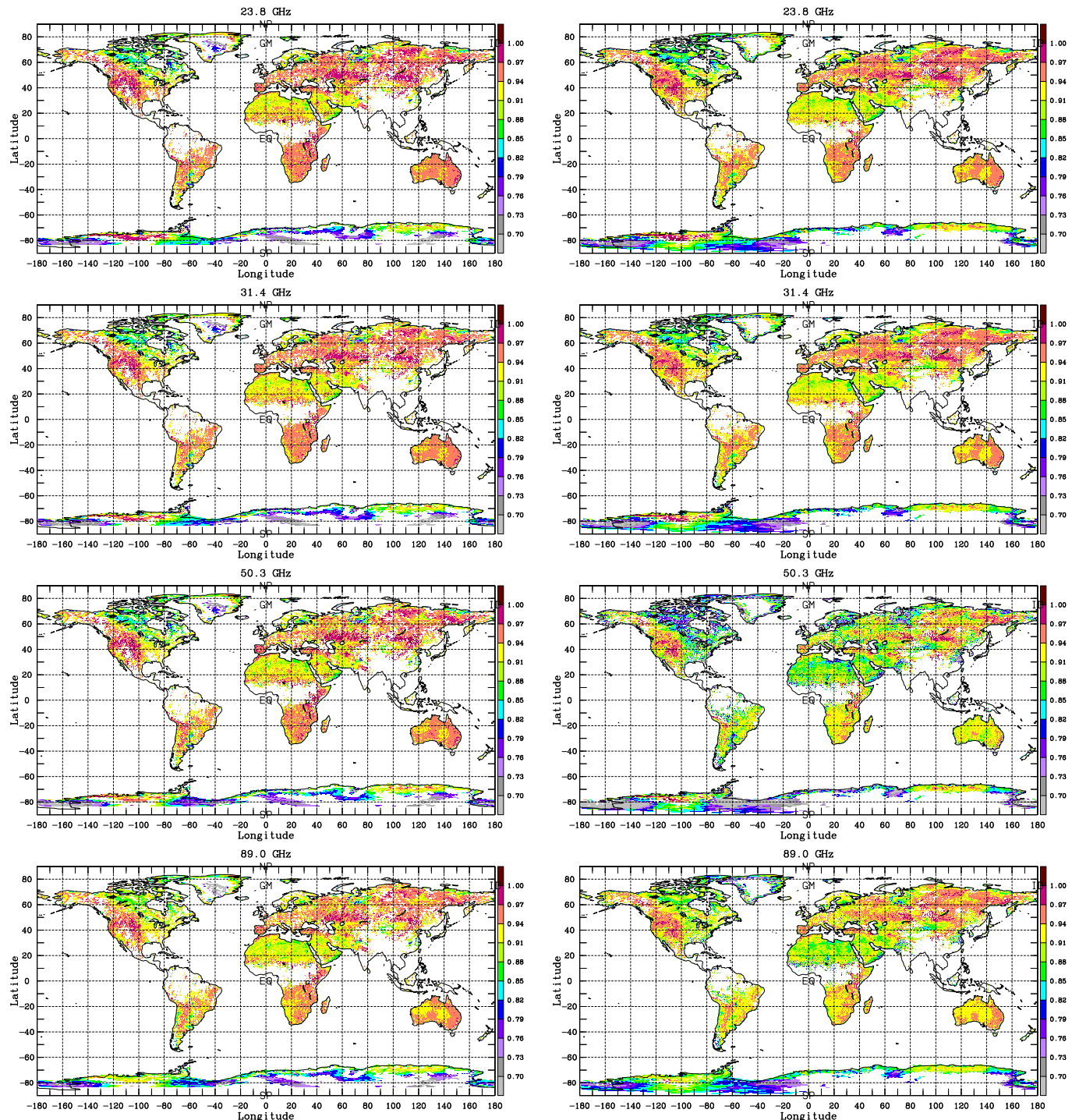


Figure 4. Angular dependence of the AMSU-A monthly mean emissivities, as directly calculated for January 2003, separated per surface types, for the four window channels. The standard deviations are indicated for each mean value (error bars). Comparison is provided with the angular and frequency fits derived from the corresponding SSM/I emissivity calculation performed at ECMWF for the same month (the middle solid line indicates the mean with the two others giving the standard deviation).

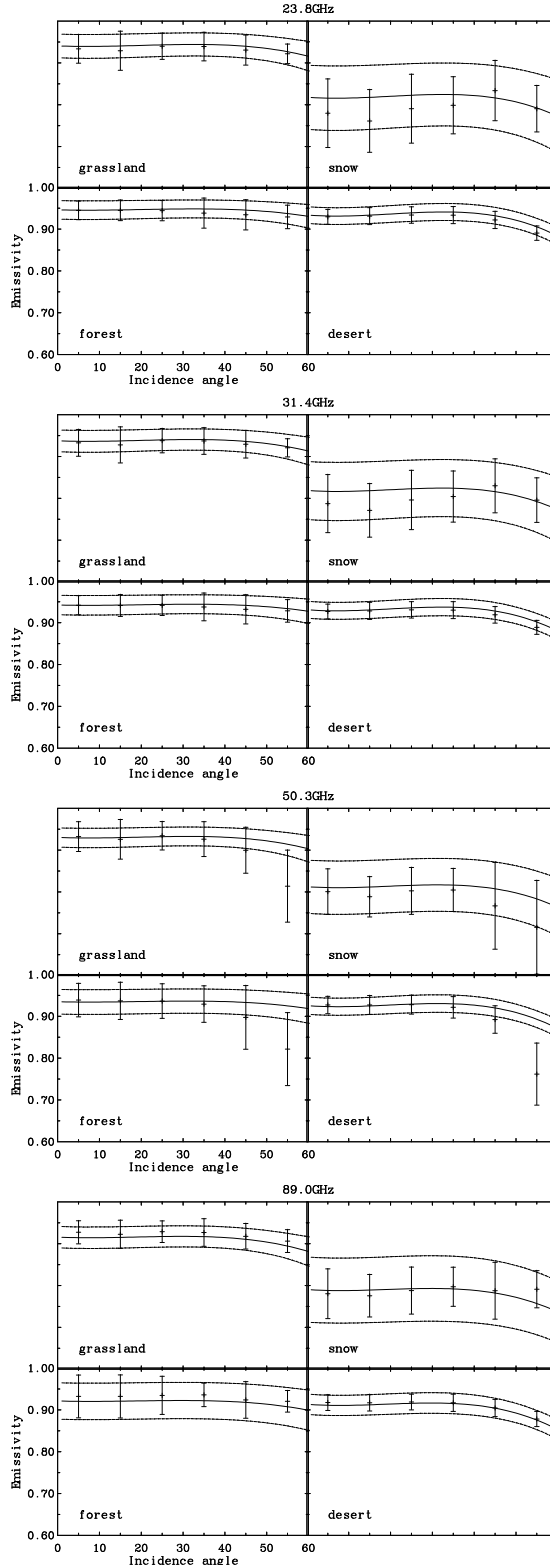


Figure 5. Frequency dependence of the NOAA-16 AMSU-A monthly mean emissivities, as directly calculated for July 2002, for incidence angles smaller than 40 degrees, separated per surface types. The standard deviations are indicated for each mean value (error bars). Comparison is provided with the angular and frequency fits derived from the corresponding SSM/I emissivity calculation performed at ECMWF for the same month (the middle solid line indicates the mean with the two others giving the standard deviation). The distinction is made between local night- and day-time observations. From top to bottom: grassland, forest, snow, and desert areas.

